Eur. J. Mineral.
2017, **29**, 663–672
Published online 31 May 2017

**Special issue dedicated to
Zdeněk Johan**

Brodtkorbite, Cu_2HgSe_2, from Příbram, Czech Republic: crystal structure and description

JIŘÍ SEJKORA[1,*], PAVEL ŠKÁCHA[1,2], FRANTIŠEK LAUFEK[3] and JAKUB PLÁŠIL[4]

[1] Department of Mineralogy and Petrology, National Museum, Cirkusová 1740, Prague 9 – Horní Počernice 193 00, Czech Republic
*Corresponding author, e-mail: jiri_sejkora@nm.cz
[2] Mining muzeum Příbram, Hynka Kličky place 293, Příbram VI 261 01, Czech Republic
[3] Czech Geological Survey, Geologická 6, 152 00 Prague 5, Czech Republic
[4] Institute of Physics ASCR, v.v.i., Na Slovance 1999/2, 182 21 Praha 8, Czech Republic

Abstract: The crystal structure and second world occurrence of the rare selenide brodtkorbite, ideally Cu_2HgSe_2, are reported in this paper. Brodtkorbite occurs in the Příbram uranium and base-metal ore district, central Bohemia (Czech Republic) as anhedral aggregates up to 150 μm across, in intergrowths with tiemannite and eucairite in a calcite gangue. Other associated minerals include berzelianite, umangite and uraninite. In reflected light, brodtkorbite is cream-white somewhat darker than the associated tiemannite and moderately pleochroic with light pink or bluish tints. Between crossed polarisers, the anisotropy is strong, with violet-grey to yellow-grey rotation tints. Reflectance values in air (R_{min}, R_{max} in %, λ nm) are 29.4–36.9 (470), 27.8–34.4 (546), 27.2–33.7 (589), 26.4–33.4 (650). Its average composition (14 electron microprobe analyses) is Ag 0.49, Hg 43.08, Cu 23.86, Se 32.25, Te 0.04, S 0.05, total 99.78 wt%. The resulting empirical formula, on the basis 5 atoms per formula unit (*apfu*), is $(Cu_{1.87}Ag_{0.02})_{\Sigma 1.89}Hg_{1.07}(Se_{2.03}S_{0.01})_{\Sigma 2.04}$. Brodtkorbite is monoclinic, *a* 7.5048(12), *b* 4.1851(9), *c* 8.0131(12) Å, β 124.430 (16)°, *V* 207.59(8) Å^3, space group $P2_1/c$, $Z = 2$. The crystal structure of brodtkorbite was solved by the direct method and refined to $R = 8.05\%$ on the basis of 416 unique reflections [$I > 3\sigma(I)$] collected on a Rigaku (Oxford Diffraction) SuperNova diffractometer with an Atlas S2 CCD detector and using Mo*K*α radiation. The crystal structure contains one special position of Hg and two general positions of Cu and Se. The crystal structure consists of layers of edge-sharing [$CuSe_4$] distorted tetrahedra where Cu atoms show a 3+1 bond scheme. The [$CuSe_4$] tetrahedra form mackinawite-like layers parallel to (100). The layers show an AA-type of stacking and are connected by linear Se–Hg–Se bonds. Each Cu atom shows three short contacts with three adjacent Cu atoms forming a pseudohexagonal net of metal-metal interactions within one layer. The brodtkorbite crystal structure shows similarities to that of imiterite (Ag_2HgS_2), but the two minerals are not isostructural.

Key-words: brodtkorbite; silver mercury selenide; selenide minerals; crystal structure; uranium deposit; Příbram; Czech Republic.

1. Introduction

Brodtkorbite is a very rare selenide of Cu and Hg, first described by Paar *et al.* (2002) from the rich selenide association of the Tumiñico selenium deposit, La Rioja, Argentina. The original crystallographic data indicated that brodtkorbite is monoclinic, space group *P*2/*n*, with *a* 7.492 Å, *b* 4.177 Å, *c* 7.239 Å, and β 114.2°, but its crystal structure was not determined. A new find of brodtkorbite at the Příbram uranium and base-metal ore district (Czech Republic) yielded material suitable for new descriptive data, which include results of the crystal structure analysis. Although the chemical composition of brodtkorbite is very simple, the synthetic phases Cu_2HgSe_2 and its sulphide analogue Cu_2HgS_2 have not yet been prepared.

2. Occurrence

Selenide mineralizations are known from several ore (especially uranium) districts of the Bohemian Massif. The most important occurrences are Bukov (Kvaček, 1973, 1979, 1987), Předbořice (Johan *et al.*, 1971a and b; Johan & Kvacek, 1971; Paar *et al.*, 2005; Bindi *et al.*, 2016), Oldřichov near Tachov (Čech & Vavřín, 1978, 1979) or Zálesí (Topa *et al.*, 2010, Sejkora *et al.*, 2011, 2012, 2014).

The Příbram ore area in central Bohemia, Czech Republic is well-known for the deposits of base-metal as well as U ores. There are two large ore districts in the Příbram ore area: the Březové Hory base-metal ore district, and the Příbram U and base-metal district. Both districts are located within the exocontact of the Permo-Carboniferous Central Bohemian

DOI: 10.1127/ejm/2017/0029-2647
0935-1221/17/0029-2647 $ 4.50

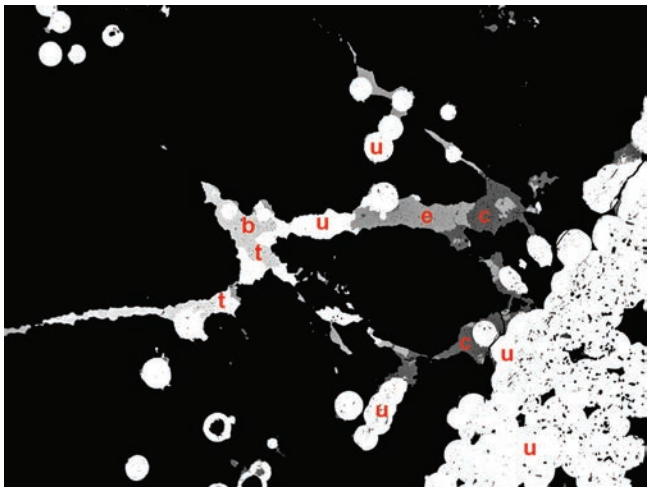

Fig. 1. Brodtkorbite (b) in association with tiemannite (t), eucairite (e), uraninite (u) and berzelianite (c). Backscatter electron (BSE) image. Horizontal field of view 1200 μm, photo J. Sejkora, P. Škácha.

Plutonic Complex with the Barrandian sedimentary unit (Ettler *et al.*, 2010). In the Příbram U and base-metal district, there are four main mineralization stages (1) siderite-sulphidic; (2) calcite; (3) calcite–uraninite; and (4) calcite-sulphidic. The selenide mineralization occurs in close association with uraninite of the calcite–uraninite mineralization, but selenides are always younger than uraninite. It is not certain whether selenides in Příbram originated at the conclusion of the calcite–uraninite stage or at the beginning of the subsequent calcite-sulphidic stage, which is mentioned by some authors. Uranium ore is represented by uraninite, coffinite and U-bearing antraxolite (pyrobitumen). The age of the U mineralization, obtained by U–Pb radiometric age determination of uraninite, is middle Permian, 275 ± 4 and 278 ± 4 Ma (Anderson, 1987). The Se–U mineralization is of low-temperature hydrothermal origin and is associated with a calcite vein tens of centimetres to several metres thick. The main ore is represented by uraninite, whereas younger antraxolite predominates in deeper parts of the deposit.

The most important source of selenide mineralization in Příbram is the Bytíz deposit, which is the predominant U deposit in Příbram, with 52% of the overall U production from the whole district. Twenty-two primary selenides species were described here in the last few years (Litochleb *et al.*, 2004; Škácha & Sejkora, 2007; Škácha *et al.*, 2009, 2014, 2015, 2016a; Škácha, 2015), including the two new minerals příbramite (Škácha *et al.*, 2017a, this issue) and bytízite (Škácha *et al.*, 2016b).

The hand specimen containing brodtkorbite was found in a dump carrying material from shaft #16 (49 67′33.028″ N, 14 05′89.919″ E), located in the Háje deposit. Shaft #16 opened mainly the middle and deeper parts of the vein system of the Háje, Bytíz and Jerusalem deposits (from 500 m down to a depth of 1800 m below the surface). The majority of the selenide-bearing material is probably derived from the Bytíz deposit (Škácha *et al.*, 2016a).

3. Physical properties

In Příbram, brodtkorbite was identified in the only fragment of carbonate gangue carrying abundant tiemannite, berzelianite, umangite and eucairite (Fig. 1). The only specimen containing brodtkorbite consists of up to 3 cm thick calcite vein, with hydrothermally altered and hematitized country rock (sample dimensions: 8 × 5 × 4 cm). Very thin green Cu secondary films (probably malachite) are present on the surface of calcite and its fractures in the proximity of selenides. Brodtkorbite forms anhedral aggregates up to 150 μm across, in intergrowths with tiemannite and eucairite, and it contains spheroidal uraninite inclusions (Fig. 2). Brodtkorbite is in part older than tiemannite, which replaces it along fractures (Fig. 3). Relatively abundant myrmekitic intergrowths of tiemannite and umangite, observed in some samples, are most probably brodtkorbite breakdown products (Fig. 4).

4. Optical properties

Samples for microscopy and other methods were prepared as polished sections using standard diamond-polishing techniques. Qualitative optical properties of brodtkorbite in reflected light were studied using a Nikon Eclipse ME600 microscope (National Museum, Prague) with a Nikon DXM1200F digital camera. Brodtkorbite from Příbram has similar properties to the type material described by Paar *et al.* (2002). It is cream-white, somewhat darker than the associated tiemannite, and moderately pleochroic with light pink or bluish tints. Internal reflections were not observed. It is strongly anisotropic, with rotation tints varying from violet-grey to yellow-grey under crossed polarisers.

Quantitative reflectance values were obtained with a Leica microscope (objective 50×) equipped with a J & M Tidas MSP 400 spectrophotometer. After careful levelling of both specimen and standard (Zeiss, WTiC), measurements were taken at intervals of 5 nm from 400 to 700 nm in air. Table 1 summarizes the data collected from the most bireflectant grains of the mineral. Data of brodtkorbite from Příbram (Fig. 5) closely match the published data for Tumiñico brodtkorbite (Paar *et al.*, 2002).

5. Chemical composition

Chemical analyses were performed using a Cameca SX100 electron microprobe (National Museum, Prague) operating in wavelength-dispersive mode (25 kV, 20 nA and 2 μm wide beam). The following standards and X-ray lines were used to minimize line overlaps: Ag (Ag*L*α), Au (Au*M*α), Bi (Bi*M*β), CdTe (Cd*L*α), Co (Co*K*α), chalcopyrite (Cu*K*α), FeS_2 (Fe*K*α, S*K*α), HgTe (Hg*M*α), NiAs (Ni*K*α, As*L*α), PbS (Pb*M*α), PbSe (Se*L*α), PbTe (Te*L*α), Sb_2S_3 (Sb*L*α), Tl (BrI) (Tl*L*α) and ZnS (Zn*K*α). Peak counting times were 20 s for all elements, and one half of the peak time for each background. Other elements, such as Au, Bi, Cd, Co, Fe, Ni, As, Pb, Sb, Tl and Zn, were found to be below the detection

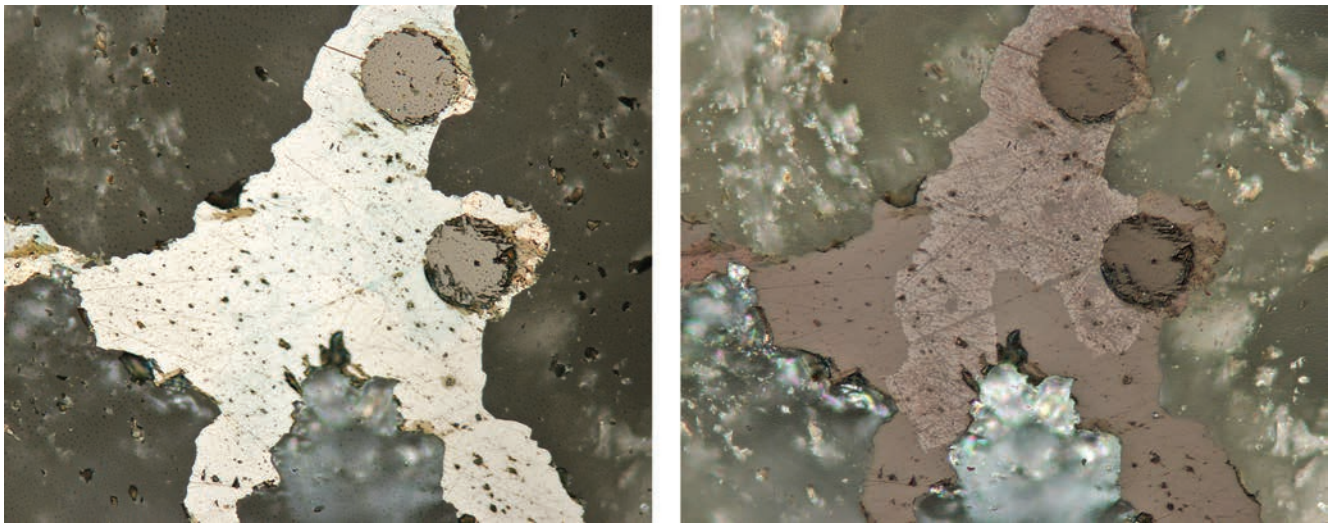

Fig. 2. (a) Brodtkorbite aggregate with bluish tint with tiemannite (yellowish) and dark spheroidal uraninite; reflected-light photomicrograph (one polariser); (b) the same brodtkorbite aggregate under crossed polarisers. Horizontal field of view 210 μm, photos P. Škácha.

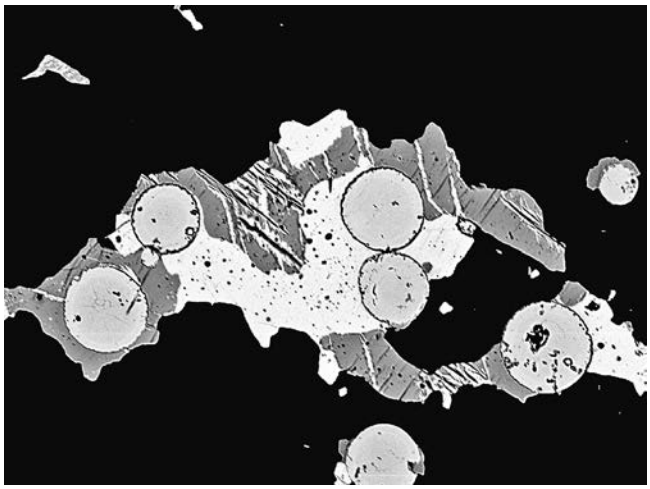

Fig. 3. Brodtkorbite (dark grey) partly replaced by later tiemannite (white) in association with spheroidal uraninite. BSE image. Horizontal field of view 300 μm, photo J. Sejkora, P. Škácha.

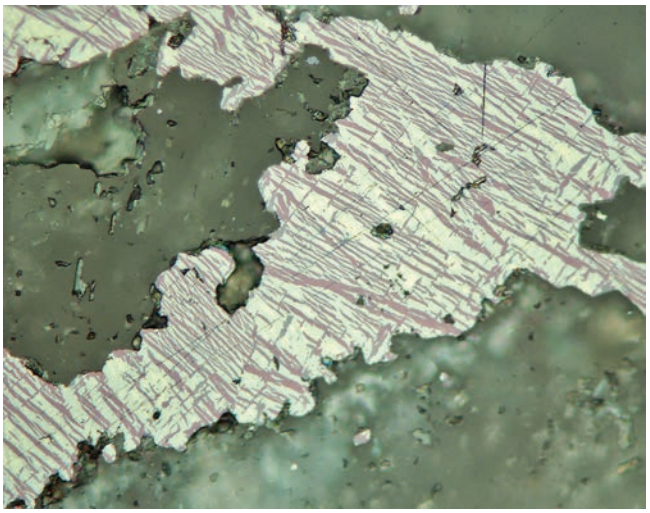

Fig. 4. Myrmekitic aggregates of tiemannite (white) and umangite (violet), probably a product of brodtkorbite breakdown. Horizontal field of view 210 μm, reflected-light photomicrograph (one polariser) J. Sejkora.

limits (0.02–0.05 wt%). Raw intensities were converted to the concentrations of elements using the "*PAP*" (Pouchou & Pichoir, 1985) matrix-correction software.

The chemical composition of brodtkorbite from Příbram (Table 2) corresponds to the ideal formula Cu_2HgSe_2. Only minor contents of Ag ($\leq$0.06 *apfu*), S ($\leq$0.01 *apfu*) and Te ($\leq$0.003 *apfu*) were observed. Although a minor Fe content was reported for the type specimen (Paar *et al.*, 2002), no Fe was found in the Příbram material. Its average empirical formula (14 analyses) based on 5 *apfu* is $(Cu_{1.87}Ag_{0.02})_{\Sigma 1.89}Hg_{1.07}(Se_{2.03}S_{0.01})_{\Sigma 2.04}$.

6. X-ray powder diffraction data

An X-ray powder diffraction pattern of brodtkorbite was obtained from hand-picked grains using a Bruker D8 Advance diffractometer equipped with solid-state 1D LynxEye detector using Cu*K*α radiation and operating at 40 kV and 40 mA (National Museum, Prague). In order to minimize the background, the powdered sample was placed on the surface of a flat silicon wafer from an acetone suspension. The powder pattern was collected using Bragg–Brentano geometry in the range 4–70° 2θ, in 0.01° steps with a counting time of 30 s/step (total duration of experiments was *ca.* 3 days). The positions and intensities of diffractions were found and refined using the Pearson VII profile-shape function of the ZDS program package (Ondruš, 1993) and the unit-cell parameters were refined by the least-squares program of Burnham (1962).

The X-ray powder diffraction pattern for brodtkorbite from Příbram (Table 3) is similar to that of the type material from Tumiñico (Paar *et al.*, 2002), obtained with a 114.6-mm

Table 1. Reflectance data of brodtkorbite from Příbram.

R_{min}/R_{max}	λ (nm)	R_{min}/R_{max}	λ (nm)
29.4/37.4	400	27.7/34.1	560
29.9/37.9	420	27.4/33.8	580
30.0/37.9	440	27.2/33.7	589
29.7/37.5	460	27.1/33.6	600
29.4/36.9	470	26.7/33.5	620
29.1/36.4	480	26.5/33.4	640
28.6/35.6	500	26.4/33.4	650
28.2/34.9	520	26.4/33.3	660
27.8/34.4	540	26.5/33.1	680
27.8/34.4	546	26.5/32.7	700

Debye–Scherrer camera; better sensitivity and resolution of data from the diffractometer led to additional diffraction peaks, yielding refined unit-cell parameters for Příbram brodtkorbite of *a* 7.5137(5), *b* 4.1840(2), *c* 8.0183(6) Å, β 124.394(3)°, *V* 208.01(4) Å^3, in excellent agreement with the single-crystal data.

7. Single-crystal X-ray diffraction

A 0.015 × 0.011 × 0.011 mm large crystal fragment of brodtkorbite extracted from the polished section was used for intensity-data collection on a Rigaku (Oxford Diffraction) SuperNova single-crystal diffractometer equipped with an Atlas S2 CCD detector utilising Mo*K*α radiation provided by the micro-focus X-ray tube and monochromatised by primary mirror optics. According to the single-crystal X-ray diffraction experiment, the studied brodtkorbite is monoclinic with $a = 7.271(3)$, $b = 4.2029(13)$, $c = 7.522(4)$ Å, $\beta = 114.19(6)°$, which is very similar to the cell in the setting proposed by Paar *et al.* (2002). This cell was later transformed to the conventional cell settings in a monoclinic space group $P2_1/c$ using the transformation matrix $(1\,0\,1/0\,1\,0/0\,0\,\bar{1})$ resulting in: $a = 7.505(1)$, $b = 4.1851(9)$, $c = 8.013(1)$ Å, $\beta = 124.43(2)°$ with $V = 207.59(8)$ Å^3, $Z = 2$. The ω rotational scans (frame width 1.0°, counting time 300 s) were adopted for the acquisition of the three-dimensional intensity data. From the total of 2777 reflections, 460 were independent and 416 classified as unique and observed with $I > 3\sigma(I)$. Corrections for background, Lorentz effects and polarisation were applied during the data reduction using the Crysalis package supplied by Rigaku. The empirical correction for absorption (spherical-harmonics) was applied leading to the dataset with R_{int} of 0.068.

The structure of brodtkorbite was solved by the charge-flipping algorithm implemented in the SHELXT program (Sheldrick, 2015). The solution provided a complete structure, which was subsequently refined by full-matrix least-squares using Jana2006 (Petříček *et al.*, 2014) based on F^2. All atoms were refined with anisotropic atomic displacement parameters. The refinement for 27 parameters converged smoothly to the final $R = 0.0811$ and $wR = 0.1729$ for 416 unique observed reflections. Details of data collection, crystallographic data and refinement are given in Table 4. Atom coordinates, displacement parameters and tentative bond-valence sums are listed in Table 5; selected interatomic distances are provided in Table 6.

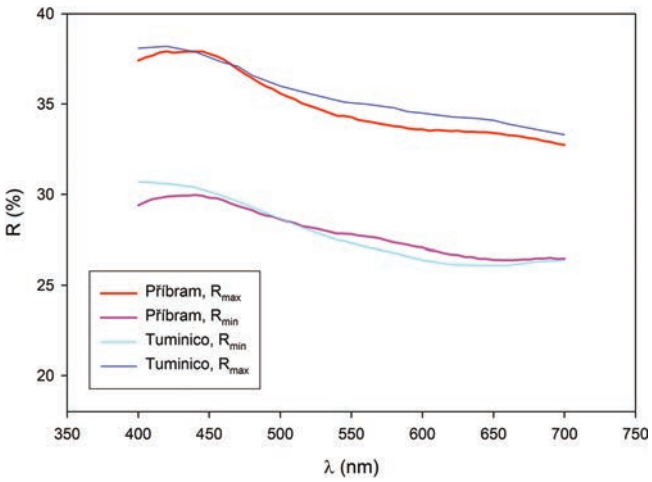

Fig. 5. Reflectance spectra in air ($R_{max.}$, R_{min}) for brodtkorbite from Příbram and Tumiñico (Paar *et al.*, 2002).

8. Crystal structure of brodtkorbite and related structures

The crystal structure of brodtkorbite contains one special position of Hg and two general positions of Cu and Se. The site-scattering experiment of using Ag entering the Cu site was tested but did not return physically realistic values, probably due to the limited quality of the diffraction data. As is indicated in Fig. 6, the Cu site displays a *quasi*-tetrahedral coordination by Se atoms with a (3 + 1) bonding scheme. The Cu site has three close contacts with Se atoms at distances ranging from 2.415 to 2.531 Å forming a trigonal base of the deformed tetrahedron. The coordination is completed by the fourth Se atom at a distance of 2.891 Å. The distortion of the [$CuSe_4$] tetrahedron is also reflected by a variation of Se–Cu–Se angles ranging from 79.2° to 119.0°, instead of being 109.47° for a regular tetrahedron. In this particular tetrahedron, the Cu atom is in a very off-centred position, with the distance between the Cu atom to the centre of the tetrahedron being 0.53 Å. The Hg atoms display typical linear coordination by two Se atoms at distances of 2.479 Å. Their coordination is further completed by four long Hg–Se distances at 3.397 Å and 3.420 Å, so the complete coordination sphere of Hg can be described as a strongly flattened octahedron. There are no short Cu–Hg interactions (<3.3 Å) in the structure of brodtkorbite.

The crystal structure of brodtkorbite is composed of layers of edge-sharing [$CuSe_4$] distorted tetrahedra running parallel to (100) (Fig. 7a). It resembles the layers of [FeS_4] tetrahedra observed in the mackinawite crystal structure (Makovicky, 2006). However, while the [FeS_4] tetrahedra in the mackinawite structure are almost perfectly regular (Lennie *et al.*, 1995), the [$CuSe_4$] tetrahedra in brodtkorbite are quite distorted. The CuSe layers show an AA-type stacking and are connected by linear Se–Hg–Se bonds. Each Cu atom also shows three short metal–metal contacts with

Table 2. Chemical composition of brodtkorbite from Příbram (wt%).

	Mean	1	2	3	4	5	6	7	8	9	10	11	12	13	14
Ag	0.49	0.20	0.27	0.18	0.68	0.17	0.20	0.41	1.26	0.19	0.94	0.33	1.35	0.36	0.37
Hg	43.08	42.89	44.38	43.71	46.32	43.69	43.83	44.58	44.60	42.41	42.72	40.61	42.71	40.75	39.92
Cu	23.86	22.72	23.01	22.74	22.85	23.11	23.10	22.40	23.42	23.90	24.62	25.23	24.64	25.74	26.51
Se	32.25	32.82	32.52	32.11	31.65	32.57	32.42	30.81	32.02	32.49	32.02	32.75	31.78	32.90	32.71
Te	0.04	0.11	0.07	0.07	0.00	0.07	0.00	0.00	0.00	0.06	0.07	0.07	0.00	0.00	0.00
S	0.05	0.00	0.07	0.00	0.07	0.05	0.05	0.08	0.08	0.05	0.07	0.08	0.05	0.06	0.06
Total	99.78	98.74	100.33	98.82	101.57	99.66	99.60	98.28	101.38	99.10	100.45	99.06	100.52	99.80	99.57
Ag	0.023	0.010	0.013	0.008	0.031	0.008	0.009	0.020	0.058	0.009	0.043	0.015	0.061	0.016	0.017
Hg	1.068	1.081	1.106	1.107	1.155	1.092	1.097	1.144	1.100	1.054	1.047	0.992	1.046	0.986	0.961
Cu	1.867	1.807	1.810	1.818	1.799	1.824	1.825	1.815	1.824	1.875	1.904	1.946	1.906	1.966	2.014
Se	2.032	2.100	2.058	2.066	2.005	2.069	2.061	2.009	2.006	2.052	1.993	2.032	1.978	2.023	1.999
Te	0.001	0.003	0.003	0.000	0.000	0.000	0.000	0.000	0.000	0.003	0.003	0.003	0.000	0.000	0.000
S	0.009	0.000	0.012	0.000	0.010	0.008	0.008	0.013	0.012	0.007	0.011	0.012	0.008	0.009	0.010

Coefficients of empirical formula were calculated on the basis of 5 *apfu*.

Table 3. X-ray powder diffraction pattern of brodtkorbite from Příbram.

h	k	l	$d_{obs.}$	$I_{obs.}$	$d_{calc.}$	$d^*_{obs.}$	$I^*_{obs.}$	h	k	l	$d_{obs.}$	$I_{obs.}$	$d_{calc.}$
1	0	0	6.201	4.6	6.200	6.259	10	2	1	2	1.6605	1.4	1.6604
1	0	$\bar{2}$	4.007	100.0	4.006	3.991	70	0	0	4	1.6541	4.3	1.6541
1	1	$\bar{1}$	3.571	57.8	3.571	3.576	50	2	2	$\bar{3}$	1.6374	3.6	1.6376
0	1	1	3.537	37.8	3.536	3.534	50	1	2	$\bar{3}$	1.6276	2.1	1.6276
1	1	0	3.468	39.7	3.468	3.476	10	4	1	$\bar{1}$	1.6095	3.6	1.6095
2	0	$\bar{2}$	3.425	81.3	3.425	3.414	50	3	2	$\bar{2}$	1.6038	4.3	1.6039
2	0	0	3.100	8.0	3.100	3.095	20	3	1	1	1.5871	1.8	1.5877
1	1	$\bar{2}$	2.894	3.3	2.894	2.887	10	1	2	2	1.5801	2.6	1.5793
2	1	$\bar{1}$	2.785	21.8	2.785	2.784	20	4	0	0	1.5500	4.4	1.5500
1	1	1	2.737	82.5	2.737	2.730	100	0	1	4	1.5379	0.3	1.5383
2	1	$\bar{2}$	2.650	6.9	2.650	2.644	10	3	1	$\bar{5}$	1.4920	7.8	1.4920
3	0	$\bar{2}$	2.4979	20.4	2.4980	2.495	30	2	1	$\bar{5}$	1.4794	2.1	1.4795
2	1	0	2.4920	20.1	2.4909			3	2	0	1.4704	2.1	1.4702
1	0	2	2.4079	57.5	2.4080	2.401	30	5	0	$\bar{4}$	1.4665	1.9	1.4664
2	1	$\bar{3}$	2.2280	64.7	2.2276	2.223	70	5	0	$\bar{2}$	1.4644	2.0	1.4644
1	1	$\bar{3}$	2.2029	22.9	2.2027	2.199	30	2	2	$\bar{4}$	1.4468	1.1	1.4468
3	1	$\bar{2}$	2.1448	9.1	2.1448	2.140	40	4	1	$\bar{5}$	1.4234	4.3	1.4233
0	2	0	2.0921	15.1	2.0920			3	2	$\bar{4}$	1.4173	3.8	1.4176
1	1	2	2.0878	34.7	2.0870			5	1	$\bar{3}$	1.4143	1.1	1.4143
3	1	$\bar{1}$	2.0786	27.2	2.0785	2.072	50	1	0	4	1.4118	1.9	1.4119
3	0	0	2.0668	3.8	2.0667			1	2	$\bar{4}$	1.4004	1.5	1.4005
1	2	$\bar{1}$	2.0013	4.5	2.0008			4	2	$\bar{2}$	1.3923	2.0	1.3924
0	2	1	1.9946	16.6	1.9947	1.989	20	4	2	$\bar{3}$	1.3869	1.6	1.3870
1	2	0	1.9821	6.8	1.9822			2	1	3	1.3709	5.1	1.3710
0	1	3	1.9514	17.7	1.9510	1.947	10	1	3	$\bar{1}$	1.3665	4.0	1.3666
3	0	$\bar{4}$	1.9278	12.7	1.9276	1.922	5						
1	0	$\bar{4}$	1.8855	24.8	1.8853	1.883	20						
1	2	$\bar{2}$	1.8542	13.2	1.8544	1.851	15						
2	0	2	1.8089	15.0	1.8090	1.803	20						
2	2	$\bar{2}$	1.7849	1.4	1.7853	1.782	3						
0	2	2	1.7680	7.3	1.7682	1.765	10						
3	1	$\bar{4}$	1.7507	6.8	1.7508	1.746	3						
2	2	0	1.7342	9.7	1.7341	1.731	10						
1	1	$\bar{4}$	1.7193	0.8	1.7189								
4	0	$\bar{4}$	1.7124	7.5	1.7123	1.711	5						
4	1	$\bar{3}$	1.6940	7.3	1.6941	1.689	20						

$d^*_{obs.}$, $I^*_{obs.}$ – X-ray powder diffraction data for brodtkorbite from Tumiñico (Paar *et al.*, 2002).

Table 4. Summary of data collection conditions and refinement parameters for brodtkorbite.

Formula	Cu_2HgSe_2
Crystal system	Monoclinic
Space group	$P2_1/c$
Unit-cell parameters: a, b, c [Å]	7.5048(12), 4.1851(9), 8.0131(12)
β [°]	124.430(16)
Unit-cell volume [Å^3]	207.59(8)
Z	2
Calculated density [g/cm^3]	7.769 (for above formula)
Crystal size [mm]	0.015 × 0.01 × 0.01
Diffractometer	Rigaku SuperNova with Atlas S2 CCD
Temperature [K]	297
Radiation, wavelength [Å]	Mo$K\alpha$, 0.71073 (50 kV, 30 mA)
θ range for data collection [°]	5.09-28.65
Limiting Miller indices	$h = -10 \rightarrow 9$, $k = -5 \rightarrow 5$, $l = -10 \rightarrow 9$
Axis, frame width (°), time per frame (s)	ω, 1.0, 150
Total reflections collected	2777
Unique reflections	490
Unique observed reflections, criterion	416, [$I > 3\sigma(I)$]
Absorption coefficient [mm^{-1}], type	64.34; empirical
T_{min}/T_{max}	0.00107/0.00825
Data completeness to θ_{max} (%), R_{int}	99.28, 0.076
Structure refinement	Full-matrix least-squares on F^2
No. of param., restraints, constraints	27, 0, 0
R, wR (obs)	0.0805, 0.1782
R, wR (all)	0.0888, 0.1811
GOF obs/all	2.78, 2.59
Weighting scheme, weights	σ, $w = 1/(\sigma^2(I) + 0.00016I^2)$
Largest diffraction peak and hole (e$^-$/Å^3)	3.95, −2.34

three adjacent Cu atoms at distances of 2.535 and 2.670 Å, respectively, forming a pseudohexagonal net of metal–metal interactions (Fig. 7b) within one layer.

The crystal structure of brodtkorbite appears to be unique; there are no exact structural analogues between similar chalcogenides. The mackinawite-type layer is a characteristic structural feature for the thalcusite–rohaite series (Makovicky *et al.*, 1980). Tetrahedral coordination of Cu has also been observed in crystal structures of ternary phases from the Tl–Cu–Se system; *e.g.*, in crookesite ($TlCu_7Se_4$; Eriksson *et al.*, 1991) and the synthetic phases $TlCu_4Se_3$ (Berger, 1987), $TlCu_5Se_3$ (Berger *et al.*, 1990) and $TlCu_3Se_2$ (Berger & Eriksson, 1990). However, in these compounds, the Tl atoms are coordinated by eight Se atoms in roughly cubic arrangement, whereas Hg atoms in brodtkorbite display a linear coordination. Imiterite, Ag_2HgS_2 (Guillou *et al.*, 1985), shows a stoichiometry that is analogous to that of brodtkorbite (Cu_2HgSe_2); both minerals exhibit the same symmetry ($P2_1/c$) and an identical sequence of occupied Wyckoff positions (*i.e.*, they are *isopontial* structures).

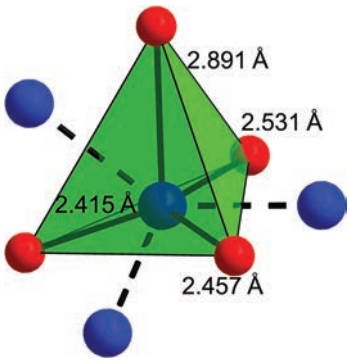

Fig. 6. *Quasi*-tetrahedral coordination of Cu in the brodtkorbite crystal structure showing Cu–Se bond distances. The Cu–Cu interactions are indicated by dashed lines.

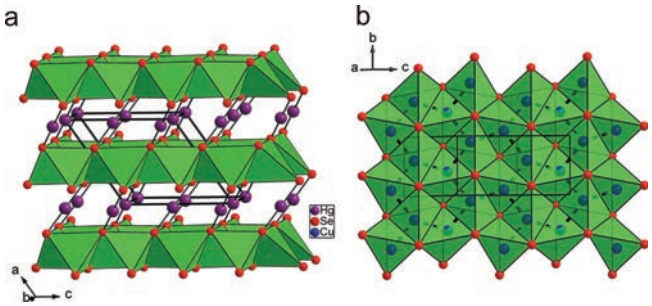

Fig. 7. (a) Polyhedral representation of the crystal structure of brodtkorbite emphasising the mackinawite-type layers of edge-sharing [$CuSe_4$] tetrahedra. The linear Se–Hg–Se bonds are indicated. (b) A (100) mackinawite-type layer of [$CuSe_4$] tetrahedra showing the pseudohexagonal net of Cu–Cu interactions.

However, both crystal structures differ to a certain extent. On one hand, a linear coordination of Hg occurs in both structures and Cu (Ag) atoms display a 3 + 1 bonding scheme by Se (S) atoms, respectively. On the other hand, the imiterite structure shows a different topology of metal–chalcogen bonds and lacks the system of metal–metal interactions found in brodtkorbite. Within the experimental study of the Hg–Cu–S system by Ollitrault-Fichet *et al.* (1984), a partial solid solution along the HgS–Cu_2S line with a limiting composition of $Cu_{2.15}Hg_{0.92}S_2$ was described. This phase is chemically very close to the brodtkorbite. However, this solid solution shows cubic symmetry and is only stable at high temperatures (>416 °C). It is not quenchable.

9. Raman spectroscopy

Raman spectra of brodtkorbite from Příbram were collected in the range 25–1800 cm^{-1} using a DXR dispersive Raman Spectrometer (Thermo Scientific) mounted on a confocal Olympus microscope (National Museum, Prague). The Raman signal was excited by a NIR 780 nm diode-pumped solid-state laser and detected by a CCD detector. The experimental parameters were: 50× objective, 10 s exposure, 100 exposures, 830 lines/mm grating, 50 μm slit spectrograph aperture, and 0.2 mW laser power level. The

Table 5. Atom positions, displacement parameters (Å^2) and bond-valence (BV) sums for brodtkorbite.

Atom	x	y	z	U_{eq}	BV
Hg	0	0.5	0.5	0.0595(8)	1.951(8)
Se	−0.2715(3)	0.8416(6)	0.2152(3)	0.0448(11)	1.697(8)
Cu	−0.4707(6)	0.9080(10)	0.3666(5)	0.0675(19)	0.721(6)

	U^{11}	U^{22}	U^{33}	U^{12}	U^{13}	U^{23}
Hg	0.0537(9)	0.0656(11)	0.0497(9)	0.0100(6)	0.0234(7)	0.0093(6)
Se	0.0445(12)	0.0489(14)	0.0418(12)	0.0002(9)	0.0247(9)	0.0004(9)
Cu	0.080(2)	0.077(2)	0.060(2)	0.0206(19)	0.0486(18)	0.0113(17)

Table 6. Interatomic distances (Å) in brodtkorbite and imiterite (Guillou *et al.*, 1985).

	Brodtkorbite		Imiterite
Hg–Se	2.479(2) (2×)	Hg–S	2.3759 (2×)
Cu–Se	2.415(6)	Ag–S	2.495
	2.456(5)		2.5996
	2.891(5)		2.6539
	2.531(5)		
Cu–Cu	2.671(6) (2×)		
	2.534(7)		

instrument was set up by a software-controlled calibration procedure using multiple Ne emission lines (wavelength calibration), multiple polystyrene Raman bands (laser-frequency calibration) and standardized white-light sources (intensity calibration). Spectral manipulations were performed using the Omnic 9 software (Thermo Scientific).

The dominant feature of the brodtkorbite spectrum (Fig. 8, Table 7) is the presence of intense vibration bands in the 220–170 cm^{-1} region. According to the literature (Nakamoto, 2009; Kharbish *et al.*, 2007, 2009; Škácha *et al.*, 2014; Števko *et al.*, 2015), these bands can be assigned to stretching vibrations of the $CuSe_4$ tetrahedra and Hg–Se bonds. As the $CuSe_4$ tetrahedra are distorted with different internal bond-lengths and form complex CuSe layers connected by linear Se–Hg–Se bonds, we were not able to determine and assign the precise character of the observed vibration bands. The most intense band at 189 cm^{-1} can be connected with vibrations of Hg–Se bonds, similar to that observed in tiemannite, HgSe (191 cm^{-1}, our study; 200–220 cm^{-1}, RRUFF R050550, R060463). The vibrations connected with Hg–S bonds are observed at 275–261 cm^{-1} (grumiplucite, $HgBi_2S_4$, Števko *et al.*, 2015), 283 cm^{-1} (imiterite, Ag_2HgS_2, our study, Fig. 9) or 255–290 cm^{-1} (cinnabar, HgS, Frost *et al.*, 2002). A substantial decrease of frequencies from X–S to X–Se bonds (about 100 cm^{-1} and more), according to Hook's rule, is described, *e.g.*, for $Nb(S/Se)_4$ and $Mo(S/Se)_4$ tetrahedra (Nakamoto, 2009) or for famatinite Cu_3SbS_4 and permingeatite Cu_3SbSe_4 (Škácha *et al.*, 2014).

Table 7. Band-components of the Raman spectrum of brodtkorbite.

Position/rel. intensity/FWHM (cm^{-1}/%/cm^{-1})	Tentative assignment
378/2/16	Overtones
197/13/6	Cu–Se and Hg–Se stretching vibrations
189/100/3	
147/19/8	Cu–Se and Hg–Se bending vibrations
103/7/5	
91/3/6	External modes (translations and librations)
83/2/6	
75/2/6	
67/3/8	
55/9/13	
42/20/8	
37/22/5	

The less intense bands of brodtkorbite in the region 160–100 cm^{-1} can be assigned to bending vibrations of Hg–Se and Cu–Se bonds and those below 100 cm^{-1} should correspond to external modes (translations and librations). The broad band at 378 cm^{-1} probably belongs to overtones.

10. Conditions of formation

Formation temperatures of the selenide mineralization of the Příbram area are similar to those at other selenide occurrences in the Czech Republic at around 100 °C. Berzelianite forms at temperatures exceeding 112 °C, and it alters to umangite at lower temperatures (Simon & Essene, 1996). Both minerals are relatively abundant in the studied selenide association. Locally, athabascaite occurs and indicates temperatures below 100 °C (Harris *et al.*, 1970). Results of a fluid-inclusion study in carbonates of the uraninite–antraxolite stage indicate crystallization temperatures in the range 140–80 °C (Žák & Dobeš, 1991). Similar temperatures (130–60 °C), based on a study of selenide mineralization and fluid inclusions, were obtained from the Tumiñico Se deposit, Argentina (Paar *et al.*, 2002).

Parasyuk *et al.* (1999) summarized the experimental study of the Cu_2Se–HgSe *quasi*-binary system. The system is of the eutectic type, and no ternary phases were detected in

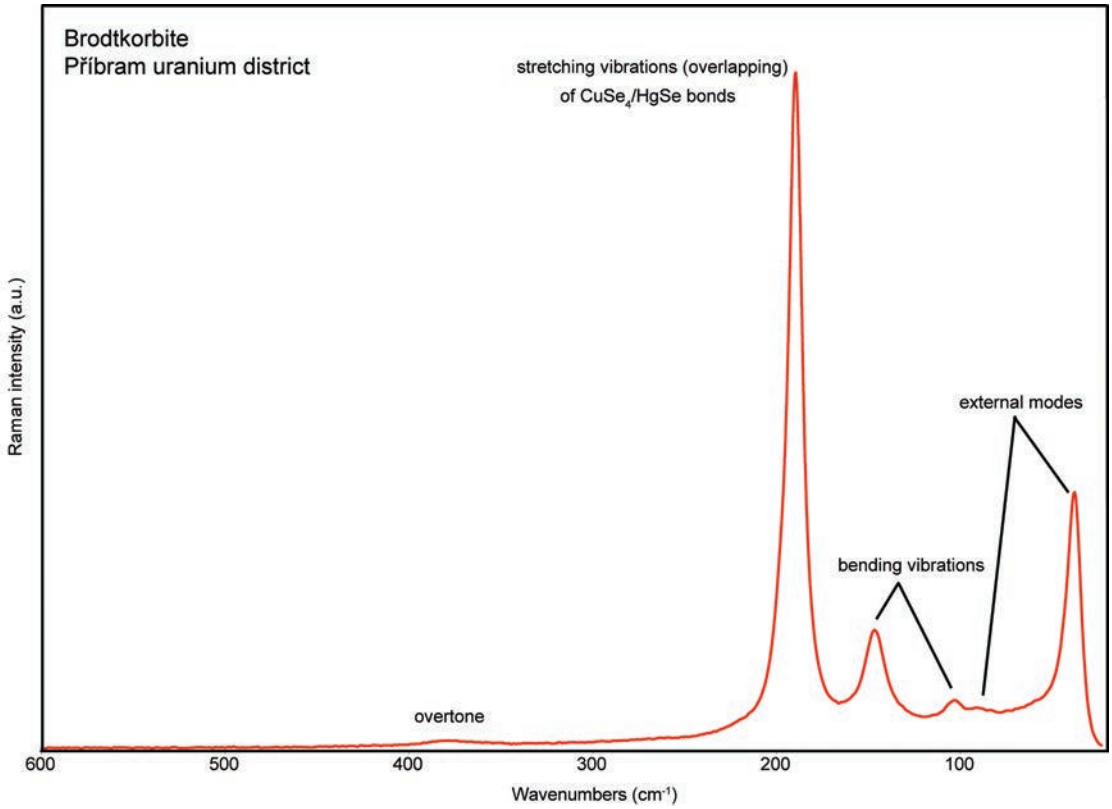

Fig. 8. Raman spectrum of brodtkorbite.

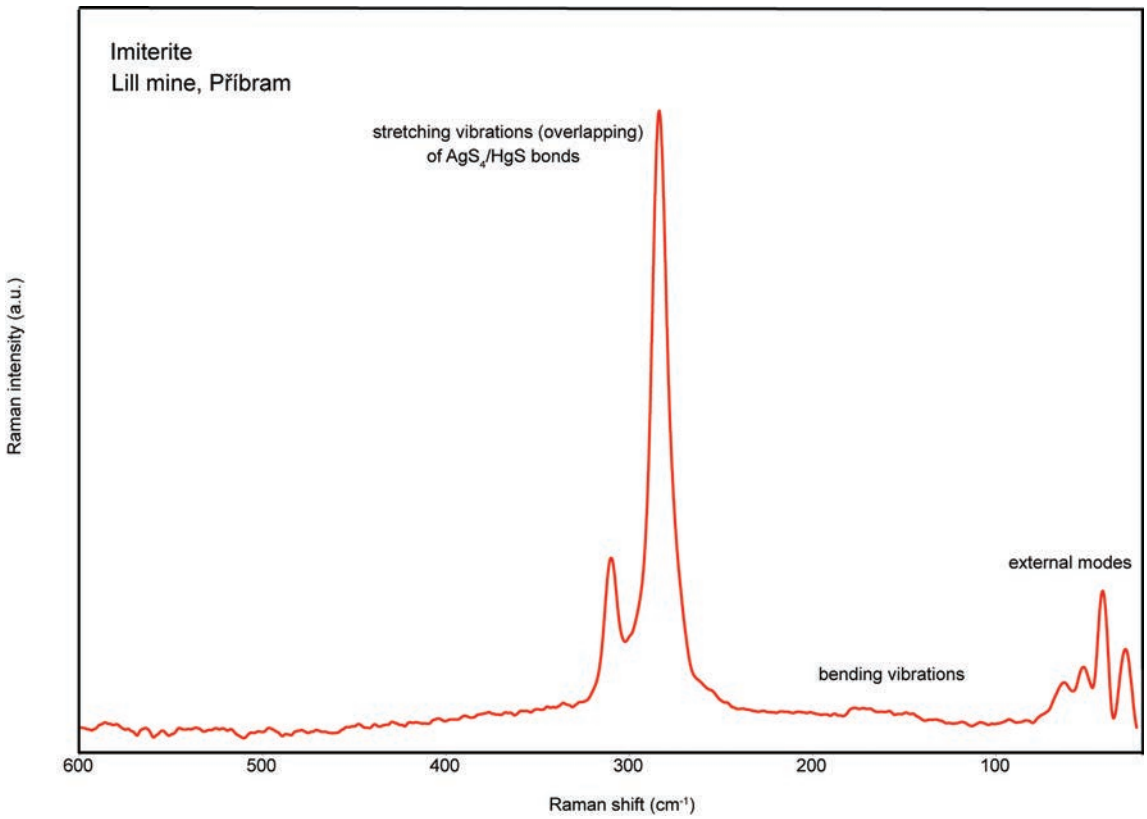

Fig. 9. Raman spectrum of imiterite, mine Lill, Příbram, Czech Republic; $Ag_{2.04}Hg_{1.01}As_{0.01}S_{1.94}$, monoclinic, *a* 4.038(1), *b* 8.006(1), *c* 6.582(1) Å, β 107.09(2)° (Plášil *et al.*, 2009).

the performed experiments. It is worth mentioning that the solubility region of Cu_2Se (α-solid solution) extends to 54 mol% HgSe at the eutectic temperature (715 °C). The solubility diminishes as the temperature decreases. The non-existence of the ordered ternary phase at temperatures close to the eutectic point also supports the formation of brodtkorbite at low temperatures.

The abundance of calcite in the gangue indicates a neutral to weakly alkaline environment of these hydrothermal fluids (Dymkov, 1985; Kvaček, 1987). The selenide mineralization is formed from hydrothermal fluids at conditions of fO_2 above the hematite–magnetite buffer, probably in the range of 5.8 log units (hematite–ferroselite univariant reaction) to 7 log units (anglesite–galena buffer) above the hematite–magnetite buffer (Simon *et al.*, 1997). Such high fO_2 values result in geochemical separation of Se from S in the hydrothermal fluids, a high Se_2/S_2 fugacity ratio and in the deposition of various selenide minerals. The quantity and variability of the selenide association which formed under oxidising hydrothermal conditions are a function of fSe_2 and reflects the concentration of available Se in solutions (Simon *et al.*, 1997).

The selenide mineralization in the Příbram U district shows variations in fSe_2 and fS_2 (Se, −12 to −18; S, −17 to −24), which are similar to those published in detail (Simon *et al.*, 1997) for "selenide-bearing uncorformity-related uranium deposits". Considering the absence of krutaite in the association we can expect an origin of the Se mineralisation at conditions with lower fSe_2 than those of the krutaite stability field, which according to the stability diagram at 100 °C (Simon *et al.*, 1997), corresponds to $\log fSe_2 < -12$ (Škácha *et al.*, 2017b).

Acknowledgements: We dedicate this paper in memory of Dr. Zdeněk Johan (1935–2016). Zdeněk Johan greatly contributed to the mineralogy of selenides and to the knowledge of the role of Se within Czech U deposits. The helpful comments of Chris Stanley and an anonymous reviewer are greatly appreciated. The research was financially supported by the project GA14-27006S of the Czech Science Foundation for PŠ and JS. Single-crystal X-ray diffraction experiments were done using instruments of the ASTRA lab established within the Operation program Prague Competitiveness – project CZ.2.16/3.1.00/24510. Support from the internal project of the Czech Geological Survey (project no. 332200) for FL is also acknowledged.

References

Anderson, E.B. (1987): Isotopic-geochronological investigation of the uranium mineralization of Czechoslovakia. Unpublished Czechoslovak Uranium Industry Report 1962-87.

Berger, R. (1987): A phase-analytical study of the Tl–Cu–Se system. *J. Solid State Chem.*, **70**, 65–70.

Berger, R. & Eriksson, L. (1990): Crystal structure refinement of monoclinic $TlCu_3Se_2$. *J. Less Common Met.*, **191**, 101–108.

Berger, R., Eriksson, L., Meerschaut, A. (1990): The crystal structure of $TlCu_5Se_3$. *J. Solid State Chem.*, **87**, 283–288.

Bindi, L., Förster, H.-J., Grundmann, G., Keutsch, F.N., Stanley, C.J. (2016): Petříčekite, IMA 2015-111. CNMNC Newsletter No. 30, April 2016, page 410. *Mineral. Mag.*, **80**, 407–413.

Burnham, C.W. (1962): Lattice constant refinement. *Carnegie Inst. Wash. Yearb.*, **61**, 132–135.

Čech, F. & Vavřín, I. (1978): Poubaite, $PbBi_2$(Se, Te, S) a new mineral. *N. Jb. Mineral. Mh.*, **1978**, 9–19.

—, — (1979): Součekite, $CuPbBi(S, Se)_3$, a new mineral of bournonite group. *N. Jb. Mineral. Mh.*, **1979**, 289–295.

Dymkov, J. (1985): Selenidy nasturan-karbonatnych žil. *in* Paragenezis mineralov uranonosnych žl. Nedra, Moscow, 153–162

Eriksson, L., Werner, P.E., Beger, R., Meerschaut, A. (1991): Structure refinement of $TlCu_7Se_4$ from powder profile data. *J. Solid State Chem.*, **90**, 61–68.

Ettler, V., Sejkora, J., Drahota, P., Litochleb, J., Pauliš, P., Zeman, J., Novák, M., Pašava, J. (2010): Příbram and Kutná Hora mining districts – from historical mining to recent environmental impact. *in* IMA 2010, Budapest. *Acta Miner. Petrol. Field Guide Ser.*, **7**, 1–23.

Frost, R.L., Martens, W.N., Kloprogge, J.T. (2002): Raman spectroscopic study of cinnabar (HgS), realgar (As_4S_4), and orpiment (As_2S_3) at 298 and 77 K. *N. Jb. Mineral. Mh.*, **2002**, 469–480.

Guillou, J.J., Monthel, J., Picot, P., Pillard, F., Protas, J., Samama, J. C. (1985): L'imitérite, Ag_2HgS_2, nouvelle espèce minérale; propriétés et structure cristalline. *Bull. Minéral.*, **108**, 457–464.

Harris, D.C., Cabri, L.J., Kaiman, S. (1970): Athabascaite: a new copper selenide mineral from Martin Lake, Saskatchewan. *Can. Mineral.*, **10**, 207–215.

Johan, Z. & Kvacek, M. (1971): La hakite, un nouveau minéral du groupe de la tétraédrite. *Bull. Soc. fr. Minéral. Cristallogr.*, **94**, 45–48.

Johan, Z., Picot, P., Pierrot, R., Kvaček, M. (1971a): La permingeatite Cu_3SbSe_4, un nouveau minéral du groupe de la luzonite. *Bull. Soc. franç. Minéral. Cristallogr.*, **94**, 162–165.

Johan, Z., Picot, P., Pierrot, R., Kvacek, M. (1971b): La fischesserite, Ag_3AuSe_2, premier séléniure d'or, isotype de la petzite. *Bull. Soc. fr. Minéral. Cristallogr.*, **94**, 381–384.

Kharbish, S., Libowitzky, E., Beran, A. (2007): The effect of As-Sb substitution in the Raman spectra of tetrahedrite-tennantite and pyrargyrite-proustite solid solution. *Eur. J. Mineral.*, **19**, 567–574.

Kharbish, S., Libowitzky, E., Beran, A. (2009): Raman spectra of isolated and interconnected pyramidal XS_3 groups (X = Sb,Bi) in stibnite, bismuthinite, kermesite, stephanite and bournonite. *Eur. J. Mineral.*, **21**, 325–333.

Kvaček, M. (1973): Selenides from the uranium deposits of western Moravia, Czechoslovakia – part 1. *Acta Univ. Carol. Geol.*, **1–2**, 23–36.

— (1979): Selenides from the uranium deposits of western Moravia, Czechoslovakia – part 2. *Acta Univ. Carol. Geol.*, **1–2**, 15–38.

— (1987): Mineralogicko – geochemická charakteristika selenidového zrudnění na uranových ložiskách Českého masivu. *in* Mineralogia uránových a s nimi súvisiacích nerastných surovín. Sborník Spišská Nová Ves, 89–95.

Lennie, A.R., Redfern, S.A.T., Schofield, P.F., Vaughan, D.J. (1995): Synthesis and Rietveld crystal structure refinement of mackinawite, tetragonal FeS. *Mineral. Mag.*, **59**, 677–683.

Litochleb, J., Sejkora, J., Šrein V. (2004): Selenides from the Bytíz deposit (Příbram uranium and base-metal district). *Bull. Mineral. Petrolog. Odd. Nár. Muz. (Praha)*, **12**, 113–123 (in Czech).

Makovicky, E. (2006): Crystal structures of sulfides and other chalcogenides. *Rev. Mineral. Geochem.*, **61**, 7–125.

Makovicky, E., Johan, Z., Karup-Møller, S. (1980): New data on bukovite, thalcusite, chalcothallite and rohaite. *N. Jahrb. Mineral. Abh.*, **138**, 122–146.

Nakamoto, K. (2009): Infrared and Raman spectra of inorganic and coordination compounds, 6th ed. John Wiley and Sons, New Jersey, 419 p.

Ollitrault-Fichet, R., Rivet, J., Flahaut, J. (1984): Diagramme de phase du système Hg–Cu–S: Étude du triangle Hg–Cu_2S–S. *J. Less Common Met.*, **96**, 49–62.

Ondruš, P. (1993): A computer program for analysis of X-ray powder diffraction patterns. *Mater. Sci. Forum, EPDIC-2, Enchede*, **133–136**, 297–300

Paar, W.H., Topa, D., Roberts, A.C., Criddle, A.J., Amann, G., Sureda, R.J. (2002): The new mineral species brodtkorbite, Cu_2HgSe_2, and the associated selenide assemblage from Tuminico, Sierra de Cacho, La Rioja, Argentina. *Can. Mineral.*, **40**, 225–237.

Paar, W.H., Topa, D., Makovický E., Culetto F.J. (2005): Milotaite, PdSbSe, a new palladium mineral, from Předbořice, Czech Republic. *Can. Mineral.*, **43**, 689–694.

Parasyuk, O.V., Olekseyuk, I.D., Marchuk, O.V. (1999): The Cu_2Se–HgSe–$SnSe_2$ system. *J. Alloys Compd.*, **287**, 197–205.

Petříček, V., Dušek, M., Palatinus, L. (2014): Crystallographic Computing System Jana 2006: general features. *Z. Krist.*, **229**, 345–352.

Plášil, J., Sejkora, J., Litochleb, J., Škácha, P. (2009): The occurrence of rare Ag–Hg sulfide – imiterite – in dump material of the Lill mine (černojamské deposit), the Březové Hory base metal ore district, Příbram (Czech Republic). *Bull. Mineral. Petrolog. Odd. Nár. Muz.,* **17**, 62–68 (in Czech with English abstract).

Pouchou, J.L., & Pichoir, F. (1985): "PAP" (πρZ) procedure for improved quantita-tive microanalysis. *in* Microbeam analysis, J. T. Armstrong, ed. San Francisco Press, California, 104–106.

Sejkora, J., Makovicky, E., Topa, D., Putz, H., Zagler, G., Plášil, J. (2011): Litochlebite, $Ag_2PbBi_4Se_8$, a new selenide mineral species from Zálesí, Czech Republic: description and crystal structure. *Can. Mineral.*, **49**, 639–650.

Sejkora, J., Plášil, J., Litochleb, J., Škácha, P., Pavlíček, R. (2012): A selenide association with macroscopic umangite from the abandoned uranium deposit Zálesí, Rychlebské hory Mountains (Czech Republic). *Bull. Mineral. Petrolog. Odd. Nár. Muz. (Praha),* **20**, 187–196 (in Czech with English abstract).

Sejkora, J., Macek, I., Škácha, P., Pauliš, P., Plášil, J., Toegel, V. (2014): An occurrence of Hg and Tl selenides at the abandoned uranium deposit Zálesí, Rychlebské hory Mountains (Czech Republic). *Bull. Mineral. Petrolog. Odd. Nár. Muz. (Praha),* **22**, 333–345 (in Czech with English abstract).

Sheldrick, G.M. (2015): SHELXT – Integrated space-group and crystal-structure determination. *Acta Crystallogr. A*, **71**, 3–8.

Simon, G. & Essene, E.J. (1996): Phase relations among selenides, sulphides, tellurides, and oxides: I. Thermodynamic properties and calculated equilibria. *Econ. Geol.*, **91**, 1183–1208.

Simon, G., Kesler, S.E., Essene, E.J. (1997): Phase relations among selenides, sulphides, tellurides, and oxides: II. Applications to selenide-bearing ore deposits. *Econ. Geol.*, **92**, 468–484.

Škácha, P. (2015): Role of the selenium in the late hydrothermal phase of the Příbram uranium region. Unpubl. PhD Thesis, 235 p (in Czech).

Škácha, P. & Sejkora, J. (2007): Arsenolamprite occurrence in the Příbram uranium and base-metal district. *Bull. Mineral. Petrolog. Odd. Nár. Muz. (Praha),* **14–15**, 131–133 (in Czech).

Škácha, P., Sejkora, J., Litochleb J., Hofman, P. (2009): Cuprostibite occurrence in the Příbram uranium and base-metal district (shaft No. 16, Příbram – Háje), Czech Republic. *Bull. Mineral. Petrolog. Odd. Nár. Muz. (Praha),* **17**, 73–78 (in Czech with English abstract).

Škácha, P., Buixaderas, E., Plášil, J., Sejkora, J., Goliáš, V., Vlček, V. (2014): Permingeatite, Cu_3SbSe_4, from Příbram (Czech Republic): description and Raman spectroscopy investigations of the luzonite-group of minerals. *Can. Mineral.*, **52**, 501–511.

Škácha, P., Plášil, J., Sejkora, J., Goliáš, V. (2015): Sulphur-rich antimonselite, $Sb_2(Se,S)_3$ in the Se-bearing mineral association from the uranium and base metal ore district Příbram, Czech Republic. *J. Geosci.*, **60**, 23–29.

Škácha, P., Sejkora, J., Palatinus, L., Makovicky, E., Plášil, J., Macek, I., Goliáš, V. (2016a): Hakite from Příbram, Czech Republic: compositional variability, crystal structure and the role in Se mineralization. *Mineral. Mag.*, **80**, 1115–1128.

Škácha, P., Sejkora, J., Plášil, J. (2016b): Bytízite, IMA 2016-044. CNMNC Newsletter No. 33, October 2016, page 1138. *Mineral. Mag.*, **80**, 1135–1144.

—, —, — (2017a): Příbramite, $CuSbSe_2$, the Se-analogue of chalcostibite, a new mineral from Příbram, Czech Republic. *Eur. J. Mineral.*, **29**, doi:10.1127/ejm/2017/0029-2623.

—, —, — (2017b): Selenium mineralization in Příbram uranium and base-metal deposit. *Minerals*, **7**, 1–56.

Števko, M., Sejkora, J., Peterec, D. (2015): Grumiplucite from the Rudňany deposit, Slovakia: a second world-occurrence and new data. *J. Geosci.*, **60**, 269–281.

Topa, D., Makovicky, E., Sejkora, J., Dittrich, H. (2010): The crystal structure of watkinsonite, $Cu_2PbBi_4Se_8$, from the Zálesí uranium deposit, Czech Republic. *Can. Mineral.*, **48**, 1109–1118.

Žák, K. & Dobeš, P. (1991): Stable isotopes and fluid inclusions in hydrothermal deposits: the Příbram ore region. *Rozpr. Čs. Akad. věd, Ř. Mat. Přír. Věd Acad. Prague*, 1–109.

Received 30 November 2016
Modified version received 10 March 2017
Accepted 28 March 2017